Appl. Phys. B 76, 87–95 (2003)
DOI: 10.1007/s00340-002-1053-y

Applied Physics B
Lasers and Optics

A. LAVROV[1,2]
A.B. UTKIN[1,3]
R. VILAR[1,✉]
A. FERNANDES[1]

Application of lidar in ultraviolet, visible and infrared ranges for early forest fire detection

[1] Departamento de Engenharia de Materiais, Instituto Superior Técnico, Av. Rovisco Pais 1, Lisbon 1049-001, Portugal
[2] Russian Science Center 'Applied Chemistry', Dobrolubova Ave. 14, St. Petersburg 197198, Russia
[3] Institute for Laser Physics, Birzhevaya 12, St. Petersburg 199034, Russia

Received: 15 May 2002/Revised version: 13 September 2002
Published online: 22 January 2003 •

ABSTRACT The efficiencies of direct lidars operating at 355, 532, 1064 and 1540-nm radiation wavelengths for early forest fire detection were compared. For each wavelength, the range for reliable smoke-plume detection was estimated on the basis of a computer simulation plume using a one-dimensional "top-hat" gas dynamic model for the calculation of the backscattering and extinction-coefficient profiles within the plume. The agreement between the predicted signal-to-noise ratio (SNR) and experimental results for 532 and 1064-nm wavelength radiation is good. The decrease of the signal-to-noise ratio with distance is maximum for 355 nm and minimum for 1064 nm. At 1540 nm, the decay of SNR with distance is slightly faster, but the SNR is higher than for other wavelengths, leading to the highest detection efficiency for the same energy of the probing laser pulse. For a burning rate of 2 kg/s and a laser beam divergence of 2.5 mr, the maximum distance for reliable detection varies between 6 and 12 km, depending on the wavelength.

PACS 42.68.Wt; 92.60.Mt

1 Introduction

Lidar is an active detection method, based on the analysis of the radiation backscattered from a target. Previous experimental and theoretical investigations have shown that lidar has considerable potential as a technique for detecting the tenuous smoke plumes produced by forest fires at an early stage of development [1–5] and presents considerable advantages for early forest fire detection in comparison with passive methods of fire surveillance based on images from the fire site or hot smoke plume, obtained in the visible or near-infrared ranges [6, 7].

Lidar detection instrumentation must be usable in inhabited areas, and the laser radiation must be eye-safe. Since the maximum permissible exposure for wavelengths in the range $400\,\text{nm} < \lambda < 1400\,\text{nm}$ is approximately three to four orders of magnitude lower than outside this range [8, 9], lidar forest fire detection is preferably carried out using radiation with a wavelength $\lambda < 400\,\text{nm}$ or $\lambda > 1400\,\text{nm}$. The third harmonic of a Nd:YAG laser (355 nm) and radiation with a wavelength in the vicinity of 1540 nm (produced by Er:glass lasers or Nd:YAG lasers with an optical parametric oscillator (OPO)) are promising candidates, since they combine the advantages of being eye-safe and high atmospheric transparency [3, 5, 8, 10, 11]. From the viewpoint of overall power efficiency, robustness and availability, lidars based on the first and second harmonics of a Nd:YAG laser (1064 and 532 nm, respectively) are also of great interest provided that the lidar can be made eye-safe. For these wavelengths, eye-safety conditions can be met by expanding the laser beam until the irradiance becomes lower than the safety threshold and/or by using low laser-pulse energy. Operation with lower-energy pulses provides opportunity for increasing the pulse repetition rate, which allows compensation for the loss of sensitivity by accumulating more lidar returns per unit time.

In this paper, which develops previous work [20], a comparative analysis of forest fire detection efficiency using lidar with different radiation wavelengths is performed, based on theoretical as well as experimental investigations. A numerical model of the interaction between the laser beam and smoke plume similar to the model previously described [20] was used to calculate the detection efficiency. The model was validated by comparison with the results of experiments carried out using the second harmonic of the Nd:YAG laser (532 nm).

2 Smoke-plume model

Calculation of the laser radiation power backscattered from a smoke plume requires a model of the smoke plume that describes the spreading of the wood-burning products in the atmosphere. In the present work, the smoke plume was simulated on the basis of a one-dimensional gas dynamic model. The wind influence was neglected.

By analogy with [1, 3, 5], it is assumed that the source term represents a circular fire site of radius R_f, with constant burning rate. The experimental data for particle size distribution (PSD) of Stith et al. [12] were used (see detailed discussion in Sect. 4).

The thermochemical aspects of the model were presented and discussed by Vilar and Lavrov in previous publications [3, 5]. Morton's "top-hat" approximation [15] is used to describe the distributions of velocity, temperature and smoke concentration in the hot plume of burning products over the fire site. The plume is assumed to possess axial symmetry with respect

✉ Fax: +351-21/841-8120, E-mail: rui.vilar@ist.utl.pt

to the z-axis, drawn in the vertical direction through the fire site centre. This is the result of neglecting wind. The velocity, temperature and particle concentration radii of the plume are assumed to be equal, and the velocity in the vertical direction U, temperature T and plume density ϱ are averaged over this radius $R_\mathrm{p} = R_\mathrm{p}(z)$,

$$\overline{U}(z) = \frac{2}{R_\mathrm{p}^2}\int_0^{R_\mathrm{p}} U(r,z) r \mathrm{d}r\,, \tag{1a}$$

$$\overline{T}(z) = \frac{2}{R_\mathrm{p}^2}\int_0^{R_\mathrm{p}} T(r,z) r \mathrm{d}r\,, \tag{1b}$$

$$\overline{\varrho}(z) = \frac{2}{R_\mathrm{p}^2}\int_0^{R_\mathrm{p}} \varrho(r,z) r \mathrm{d}r\,, \tag{1c}$$

where r is the coordinate in the radial direction. The "top-hat" approximation also implies that the molar mass of the gas of the hot plume is equal to that of air, and pressure equilibrium is achieved, so within the framework of the ideal-gas equation of state one can write

$$\overline{\varrho}\,\overline{T} = \varrho_\mathrm{a} T_\mathrm{a}\,, \tag{2}$$

where the index a denotes the corresponding values for ambient air. This enables a normalised temperature parameter to be defined as

$$\theta(z) = \frac{\varrho_\mathrm{a} - \overline{\varrho}}{\overline{\varrho}} g = \frac{\overline{T} - T_\mathrm{a}}{T_\mathrm{a}} g\,, \tag{3}$$

where g is gravitational acceleration. As a result, the plume parameters for a steady-state combustion process are defined by the system of ordinary differential equations

$$\begin{aligned}
&\frac{\mathrm{d}}{\mathrm{d}z}(\overline{\varrho} R_\mathrm{p}^2 \overline{U}) = 2\varrho_\mathrm{a} E \overline{U} R_\mathrm{p}\,,\\
&\frac{\mathrm{d}}{\mathrm{d}z}(\overline{\varrho} R_\mathrm{p}^2 \overline{U}^2) = \overline{\varrho}\theta R_\mathrm{p}^2\,,\\
&\frac{\mathrm{d}}{\mathrm{d}z}(\overline{\varrho}\theta R_\mathrm{p}^2 \overline{U}) = 0\,,
\end{aligned} \tag{4}$$

where E is the entrainment coefficient. According to Morton et al. [15, 16], E is defined by the quasi-empirical equation

$$E = 0.12\frac{\overline{\varrho}}{\varrho_\mathrm{a}}\,. \tag{5}$$

For given values of the fire site radius R_f and burning rate, which identify the initial values of velocity and temperature (see Lavrov and Vilar [3, 5]), the system of (4) can be solved using an explicit finite-difference scheme. The solution yields the density and cross-section radius distributions ($\overline{\varrho}(z)$ and $R_\mathrm{p}(z)$, respectively) over the plume height. In the subsequent treatment, these values are used for the definition of the distribution of the smoke particle concentration over the plume volume, required to calculate the extinction and backscattering coefficients.

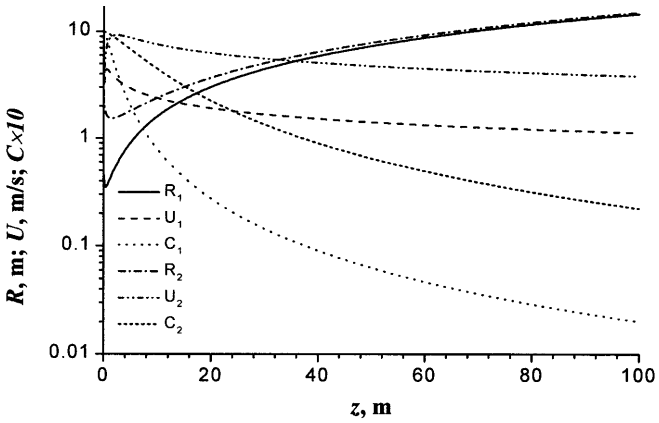

FIGURE 1 Variation of the smoke plume radius R, velocity U and relative ash density C with the distance from the ground z. Burning rate 0.05 kg/s and fire radius 0.5 m (1c) and burning rate 2 kg/s and fire radius 2.5 m (2)

The variation of the smoke-plume radius, particle velocity and relative ash density as a function of the distance to the ground for two values of the burning rate is presented in Fig. 1. As a result of the strong buoyancy forces near the ground [15], where the plume density is a minimum, a maximum in the velocity and a minimum in the smoke-plume radius occur.

The influence of wind was neglected in the calculations. The error in the smoke-plume radius and particle concentration resulting from this simplification was evaluated by comparing the model predictions with experimental data of Askari et al. [17]. These authors found experimentally that, for a jet of CH_4 with a radius of 0.075 m and a wind velocity of 5.5 m/s, the plume radius and relative particle concentration at a distance to the ground of 4.8 m were 1.4 m and 0.107, in moderately good agreement with the prediction of the model (1.19 m and 0.081, respectively) This result confirms that the influence of wind can be neglected.

3 Calculation of signal-to-noise ratio

Calculations were performed for radiation with 355, 532, 1064 and 1540-nm wavelengths in order to investigate their suitability for forest fire detection. From the viewpoint of detection efficiency, photomultipliers (PMTs) are the most advantageous detectors for lidars operating at 355 and 532 nm, while avalanche photodiodes (APD) are more efficient for 1540-nm detection. Both types of detector may be used for a 1064-nm lidar, but, in practice, photomultipliers in general are used. For this reason, a PMT detector was chosen for this wavelength in the calculations. The power collected by the lidar receiver is given by the lidar equation [18]:

$$P = E_\mathrm{l}\frac{c\pi D^2}{8R^2}\tau_\mathrm{rec}\tau_\mathrm{tr}\exp\left(-2\int_0^R \alpha(R')\mathrm{d}R'\right)\langle\beta(R)\rangle\,, \tag{6}$$

where E_l is the laser pulse energy, c the speed of light, D the diameter of the receiver's entrance pupil, R the distance, τ_rec and τ_tr the receiver and transmitter efficiencies, α the extinction coefficient, and $\langle\beta\rangle$ the mean smoke-plume backscattering coefficient. According to Andreucci and Arbolino [1, 2] and Measures [18], the equation for the signal-to-noise ratio

Distance to fire (km)	3.9	3.9	3.9	4.7	4.7	4.7	4.7	6.5	6.5
Wavelength (μm)	1.064	0.532	0.532	0.532	0.532	1.064	0.532	0.532	0.532
SNR′ experiment	90	70	130	23	32	8	89	49	160
SNR′ calculation	65	40	58	7	10	13	114	21	49

TABLE 1 Comparison between calculated and experimental [20] values of SNR′

for a PMT detector is

$$\mathrm{SNR_p} = \frac{I_{\mathrm{sig}} G}{\sqrt{2\,\mathrm{e} G^2 F B (I_{\mathrm{sig}} + I_{\mathrm{bgnd}} + I_{\mathrm{dark}})}}\,, \tag{7}$$

where $B = (2t_{\mathrm{d}})^{-1}$ is the effective bandwidth, t_{d} is the integration period (time during which a single point of the lidar signal is measured [18]), $I_{\mathrm{sig}} = \eta P$ is the PMT signal current corresponding to the received radiation power P, η is the detector responsivity, G is the photomultiplier gain, e is the electron charge, $I_{\mathrm{bgnd}} = \eta P_{\mathrm{b}}$ is the noise current defined by the received background solar radiation of power P_{b}, I_{dark} is the anode dark current, and F is a noise factor associated with the gain. For most photomultipliers $F \approx 1$, and this factor can be omitted [18].

According to Vilar and Lavrov [3, 5], Youmans et al. [10], and Overbeck et al. [19], the expression for the signal-to-noise ratio of a detector based on an avalanche photodiode takes the form

$$\mathrm{SNR_A} = \frac{P_{\mathrm{sig}}}{P_{\mathrm{T}} + P_{\mathrm{amp}} + P_{\mathrm{dark}} + P_{\mathrm{shot}} + P_{\mathrm{bgnd}}}\,, \tag{8}$$

where P_{sig} is the power of the output electric signal, P_{T} the thermal noise power, P_{amp} the power of the electronic amplifier noise, P_{dark} the power of the detector noise due to dark current, P_{shot} the signal shot-noise power, and P_{bgnd} the background illumination shot-noise power. Explicit equations for the terms in the denominator of (8) were presented in previous publications [3, 5].

Smoke plumes resulting from forest fires are compact targets, which manifest themselves in a lidar signal by narrow peaks. As a result, the most appropriate measure of the detection efficiency is the ratio between the peak signal value and the background noise in the vicinity of the peak [20]. To underline the difference between this ratio and the SNR defined by (7) or (8), the former ratio will henceforth be denoted by SNR′. The value of SNR′ can be theoretically estimated within the framework of the above considerations for SNR by calculating the denominator of (7) and (8) for the background signal level only. With this aim, the background signal was calculated on the basis of the atmospheric-aerosol backscattering coefficient, which, in turn, was estimated based on the extinction coefficient values. The ratio of the extinction coefficient to the aerosol backscattering coefficient, S, was assumed to be 30 sr on the basis of experimental [21] and numerical [22] data. This estimation corresponds to a minimum but realistic value that allows the calculation of a maximum for the Mie aerosol backscattering coefficient and minima for the signal-to-noise ratio and for the distance of reliable detection. In general, the actual detection range will be larger.

Despite the wide variability in smoke-particle shape, in the computation of optical scattering they were considered to be spheres, as suggested by Martins et al. [24]. Accordingly, Mie theory was applied. To evaluate the model, the calculated values of SNR′ were compared with experimental data [20] using the percentage of wood that is transformed into particles in the combustion process (WTP) as a fitting parameter. According to Stith et al. [12] and Patterson et al. [23], WTP varies in the range 0.2 to 2%. In the present work, the minimum discrepancy between theoretical and experimental values was achieved for WTP = 0.3% (Table 1). This value was used in the numerical calculations.

4 Detection of plume by a 0.532-μm lidar and estimation of smoke-particle concentration

The experiments required to validate the model were carried out using a lidar whose parameters are listed in Table 2. The fireplace was a 0.75-ha square of shrub land with a height of vegetation of about 1 m. The distance between the plume and the lidar was about 2.5 km.

The distribution of the extinction coefficient along the beam propagation direction in the smoke plume was calculated from the lidar signal using Klett's inversion method [25]. To perform the calculations, the background must be eliminated from the lidar signal. It is also necessary to know the extinction coefficient, $\alpha_{\mathrm{fin}} = \alpha(R_{\mathrm{fin}})$, at the farthest point, $R = R_{\mathrm{fin}}$, of the segment to be processed. The backscattering coefficient is assumed to be proportional to α^k, k = constant, and the profile of the extinction coefficient along the probing laser beam is restored from the logarithmic range-adjusted

Parameter	Notation	Units	Value
Q-switched Nd:YAG laser			
Repetition rate used		Hz	12
Pulse duration	t_{p}	ns	10
Beam divergence	–	mr	< 0.5
Operating wavelengths	λ	nm	532
Maximm pulse energy	E_{l}	mJ	30
Total transmitter efficiency	τ_{T}	%	90
Receiver			
Cassegrainian telescope, lens diameter 30 cm, focal length 156.2 cm			
Effective area	A_{r}	m^2	0.0678
Full angle of field of view	γ	mr	0.9
Efficiency	τ_{R}	%	64
Bandwidth	B_{f}	nm	4.8
Photomultiplier			
Dark current	I_{dark}	A	4×10^{-7}
Gain	G	–	$\sim 10^5$
Photocathode responsivity	η	$\mathrm{mA\,W^{-1}}$	0.7
Data acquisition system			
Distance		km	1–30
Detection length	$\frac{ct_{\mathrm{d}}}{2}$	m	6
On-board data buffer		kbytes	64
Background solar radiance		$\mathrm{W\,m^{-2}\,sr^{-1}\,\mu m^{-1}}$	120

TABLE 2 Characteristics of the lidar set-up and background solar radiation

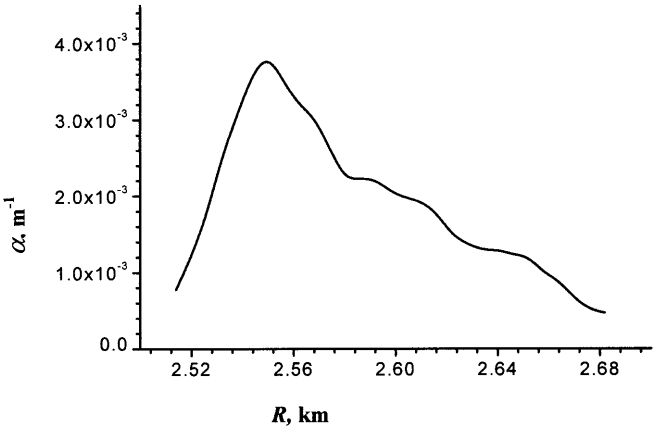

FIGURE 2 Variation of the extinction coefficient α along the laser pulse trajectory R in the smoke plume, calculated from a lidar signal using the Klett inversion method. The boundary value of the extinction coefficient is 2.5×10^{-4} m^{-1}

signal $S(R) = \ln\left(\frac{R^2 P(R)}{R_{\text{fin}}^2 P(R_{\text{fin}})}\right)$ as follows:

$$\alpha(R) = \frac{\exp(k^{-1} S(R))}{\alpha_{\text{fin}}^{-1} + 2k^{-1} \int_R^{R_{\text{fin}}} \exp(k^{-1} S(R'))\mathrm{d}R'} . \quad (9)$$

The main contribution to the extinction and backscattering coefficients in the plume comes from smoke particles. As a result, both β and α are proportional to the particle concentration in the smoke, and in the dependence $\beta \sim \alpha^k$, the choice for k is unity.

Background correction was performed by subtracting a constant background calculated by averaging the values of the last 50 points of the raw lidar signal to all points in the signal [26]. According to Klett's inversion method [25], the initial value of the extinction coefficient must be taken at a point located in a smoke-free area behind the plume. This corresponds to the extinction of a clear atmosphere and was estimated as 2.6×10^{-4} m^{-1} on the basis of Nilsson's computations for a visibility of 15 km [27]. The distribution of the extinction coefficient in the smoke plume, calculated from the lidar signal, is shown in Fig. 2. The smoke plume is located in the segment between 2510 and 2680 m and the maximum value of the extinction coefficient is $\alpha_{\max} \approx 4 \times 10^{-3}$ m^{-1}. The point corresponding to the maximum of the extinction coefficient, (i.e. the maximum of the smoke particle concentration), is shifted towards the lidar direction with respect to the middle of the smoke distribution interval because during the experiment the wind was blowing from the lidar to the fire site. As mentioned in the literature [28], the highest particle concentration zone in the smoke plume is located upwind. The variation of α_{fin} within a range of $\pm 25\%$ causes a variation of $\alpha_{\max}$ within a range $\pm 20\%$. Such a dramatic dependence of $\alpha_{\max}$ on α_{fin} results from the fact that the optical depth of the smoke plume under consideration in the probing region is not too large [29].

To estimate the particle concentration corresponding to an extinction coefficient $\alpha_{\max} \approx 4 \times 10^{-3}$ m^{-1}, the Wiscombe Fortran code for Mie scattering calculations [30] was used. The particle size distribution in wood-burning smoke was measured by Stith et al. [12], de Vries and den Breejen [13], and Hueglin et al. [14]. The experimental mean particle radii and the backscattering coefficients for different wavelengths are given in Table 3. The values of the backscattering coefficient calculated using the results of Stith et al. [12] turned out to be intermediate between those calculated using de Vries and den Breejen [13] and Hueglin et al. [14] data, and were selected as the input for the following calculations. A value of $n_1 \approx 3.7 \times 10^{11}$ m^{-3} was obtained for the maximum particle concentration. This value can be compared with an estimation based on the one-dimensional gas dynamic model developed in Sect. 3.

In the field experiments, the instantaneous fire front and area present a complicated shape, which depends on the fuel load, wind direction, ground profile and other factors. To simplify the problem, a circular fire spot with the same area and constant fuel load as the experimental fire was used for the calculations. According to Viegas et al. [31], Fernandes [32], and Cruz and Viegas [33], the fuel load of shrub in the experimental fire site was about 1.5 kg/m^2.

The estimated fire and plume parameters (fire area, fire duration, fuel load, area burned per unit time, radius of the smoke-plume equivalent circle and relative particle density at the intersection point with the probing laser beam) are presented in Table 4. The laser beam crossed the plume at a height of 330 m. The calculations developed on the basis of (4) show that the plume diameter at 330 m was about 100 m, which is

Reference	Mean radius (nm)	Operating wavelength (nm) 355	532	1064	1540
		Backscattering coefficient (m^{-1} sr^{-1})			
Stith et al. [12]	60	1.1×10^{-2}	6.6×10^{-3}	2.5×10^{-3}	2×10^{-3}
de Vries and den Breejen [13]	90	3.5×10^{-3}	3.1×10^{-3}	2.2×10^{-3}	1.5×10^{-3}
Hueglin et al. [14]	260	1.2×10^{-2}	9.7×10^{-3}	8×10^{-3}	4.4×10^{-3}

TABLE 3 Mean particle radii and corresponding backscattering coefficients

Fire duration (s)	Fire area (m^2)	Fuel load (kg/m^2)	Area burned per unit time (m^2/s)	Radius of equivalent circle (m)	Fuel burned per unit time (kg/s)	Estimated relative ash density in the area of laser beam (with respect to the plume base). $z_b = 330$ m	Smoke plume radius in the site of intersection with laser beam (m)
900	6970	1.5	7.7	1.6	11.6	0.01	98

TABLE 4 Main parameters of the fire and the smoke plume. z_b is the height at which the laser beam illuminates the smoke plume

in agreement with the value calculated from the lidar signals (120 m). The smoke particle concentration, calculated on the basis of (4), is $n_2 \approx 2.6 \times 10^{11}\ \mathrm{m}^{-3}$. This value agrees reasonably well with the value n_1 obtained by processing of the experimental lidar signal.

5 Choice of lidar, plume, and atmosphere parameters for numerical investigation

The parameters used in the calculations were found in the literature or result from previous work [3, 5, 20]. The lidar, plume and atmosphere characteristics used are presented in Table 5. The plume backscattering coefficient for various wavelengths was calculated on the basis of the particle size distribution measured by Stith [12], using a program for the calculation of Mie backscattering developed by Lavrov and Vilar [3, 5].

To achieve maximum lidar efficiency, a radiation detector with the required responsivity must be selected. For lidars operating at 355, 532, and 1064 nm, the best performance is achieved using PMTs with bialcali, multialcali, and Ag-O-Cs photocathodes, respectively. For 1540-nm lidar, the best choice of detector is an InGaAs APD with a gain of 20 and a noise excess factor of 10 [10, 19]. The extinction coefficients were estimated on the basis of Nilsson's [27] numerical results for a visibility of 15 km. This visibility is typical in Mediterranean regions during the summer and dry weather, when forest fires are likely to occur [34].

The background solar radiance was estimated on the basis assumed data of Youmans et al. [10] and Pratt [35]. For lidars operating at 1064 and 1540 nm, the pulse energy was taken to be 100 mJ. Following Althausen et al. [21], it is assumed that for this energy at the fundamental wavelength, the laser pulse energies at 532 and 355 nm will be 30 and 10 mJ, respectively.

To minimise scanning time, the solid angle covered with one laser pulse must be maximised. For better detection efficiency, the diameter of the laser beam on the target must be approximately equal to the target diameter. This is why, to test the influence of the divergence of the laser beam, divergences of 2.5 mr (narrow-scan mode) and 10 mr (wide-scan mode) were selected. For an Nd:YAG laser this requires the use of a variable beam expander, because even the narrow-scan mode has a larger divergence than the natural divergence (≈ 0.5 mr). Experimental data of Georgiou, Musset and Boquillon [36] and Wu, Myers, and Myers [37] show that the best currently available 1540-nm Er:glass lasers have a divergence of about 10 mr. We assume that a divergence of 2.5 mr will be achieved in the near future.

Independently of the type of laser, the following values were used: receiver optics diameter: 0.2 m, transmitter and receiver efficiencies: 0.9 and 0.8, respectively, receiver optical bandwidth: 2 nm. The receiver field of view corresponds to the laser beam divergence. Table 5 also presents data for maximum permissible single-pulse exposure [8, 9] and eye-safe distance for the wavelengths of interest. It should be emphasised that for 532 and 1064 nm, the eye-safe distance is large.

6 Results of calculations

Based on previous experimental results [20], it was assumed that for reliable detection, the signal-to-noise ratio (SNR′) should not be less than five. The dependence of SNR′ on distance for lidars of various wavelengths and for various operating conditions is shown in Figs. 3 to 5. When a PMT is used for detection, the slope of the curve SNR′(R) is largest for $\lambda = 355$ nm and smallest for $\lambda = 1064$ nm. This is due to the fact that the equation for the power collected by the lidar (6) includes the product of the extinction and the distance

Parameter	Operating wavelength (nm) 355	532	1064	1540
Transmitter:				
Energy at main harmonic (mJ)	100	100	100	100
Efficiency of conversion of wavelength of radiation (%)	10	30	–	–
Laser energy (mJ)	10	30	100	100
Receiver:				
Detector type	PMT	PMT	PMT	APD
Photocathode material of PMT	Bialcali	Multialcali	Ag-O-Cs	–
Detector responsivity, A/W	0.04	0.04	0.0004	1
Detector gain	5×10^6	5×10^6	2×10^6	20
PMT anode dark current, A	10^{-7}	10^{-7}	8×10^{-7}	–
APD dark current, A	–	–	–	10^{-7}
Detector noise factor	1	–	–	10
APD load resistance (Ω)	–	–	–	50
Solar radiance, atmosphere and plume parameters:				
Plume backscattering coefficient ($\mathrm{m}^{-1}\,\mathrm{sr}^{-1}$)	1.1×10^{-2}	6.6×10^{-3}	2.5×10^{-3}	2×10^{-3}
Background solar radiance ($\mathrm{W\,m^{-2}\,sr^{-1}\,\mu m^{-1}}$)	30	120	50	22
Rayleigh scattering coefficient (m^{-1})	8×10^{-5}	1×10^{-5}	≈ 0	≈ 0
Aerosol extinction coefficient (m^{-1})	3×10^{-4}	2.5×10^{-4}	1.5×10^{-4}	1×10^{-4}
Total extinction coefficient (m^{-1})	3.8×10^{-4}	2.6×10^{-4}	1.5×10^{-4}	1×10^{-4}
Maximum permissible single-pulse exposure and eye-safe distance:				
Maximum permissible single pulse exposure ($\mathrm{J/m^2}$)	60	0.005	0.03	100
Eye-safe distance (m) $\gamma = 2.5$ mr	6	1100	820	14
$\gamma = 10$ mr	2	280	210	4

TABLE 5 Lidar parameters used in the calculation

in the exponent. Since the air extinction is less for greater wavelengths (Table 5), the slope of SNR′(R) increases. For a lidar with an APD, the slope of the SNR′ curve is larger than the slope of the SNR′ curve for a lidar with a PMT as, in this case, SNR′ is a quadratic function of the received optical power [3, 19].

The relative positions of the SNR′ curves depend on detection parameters such as the air extinction coefficient, smoke-plume backscattering coefficient, and detector responsivity. The backscattering coefficient itself is defined by the particle concentration, which depends strongly on the height z_b at which the laser beam illuminates the smoke plume. Calculations were carried out for $z_b = 0$ (intersection immediately above the ground), 15 and 100 m, the latter situation being typical of fire-detection applications. The particle concentration, average smoke-plume backscattering coefficient and power collected by the lidar receiver decrease with increasing z_b while all other factors remain similar.

The lidar spatial resolution is limited by the effective laser pulse length $ct_p/2$ (equal to 1.5 and 3 m for Nd:YAG and Er:glass lasers, respectively), and as the minimum reasonable value for the integration period t_d is equal to t_p, the effective detection length, $ct_d/2$, is also equal to 1.5 or 3 m. Analysis of the detection geometry shows that when the smoke plume is wider than the effective detection length, the integration period is longer than the pulse duration. The calculated plume diameters for the situations of interest are presented in Table 6. Except for a burning rate of 0.05 kg/s and $z_b = 0$, the plume diameter exceeds 3 m. Consequently, if the integration period increases but the effective detection length does not exceed the plume diameter, the β of the smoke plume, the power collected by the lidar and the nominators in the two SNR equations (1c) and (2) do not change. Simultaneously, the corresponding denominators diminish because the integration period increases and the effective bandwidth de-

Fuel burned per unit time (kg/s)	Plume diameter (m) $z_b = 0$	$z_b = 15$ m	$z_b = 100$ m
0.05	1	4.6	29
2.0	5	6	30
	Diameter of the laser beam (m)		
	$\gamma = 2.5$ mr		$\gamma = 10$ mr
$R = 2$ km	$R = 8$ km	$R = 2$ km	$R = 8$ km
5	20	20	80

TABLE 6 Plume and laser beam parameters used in the calculations

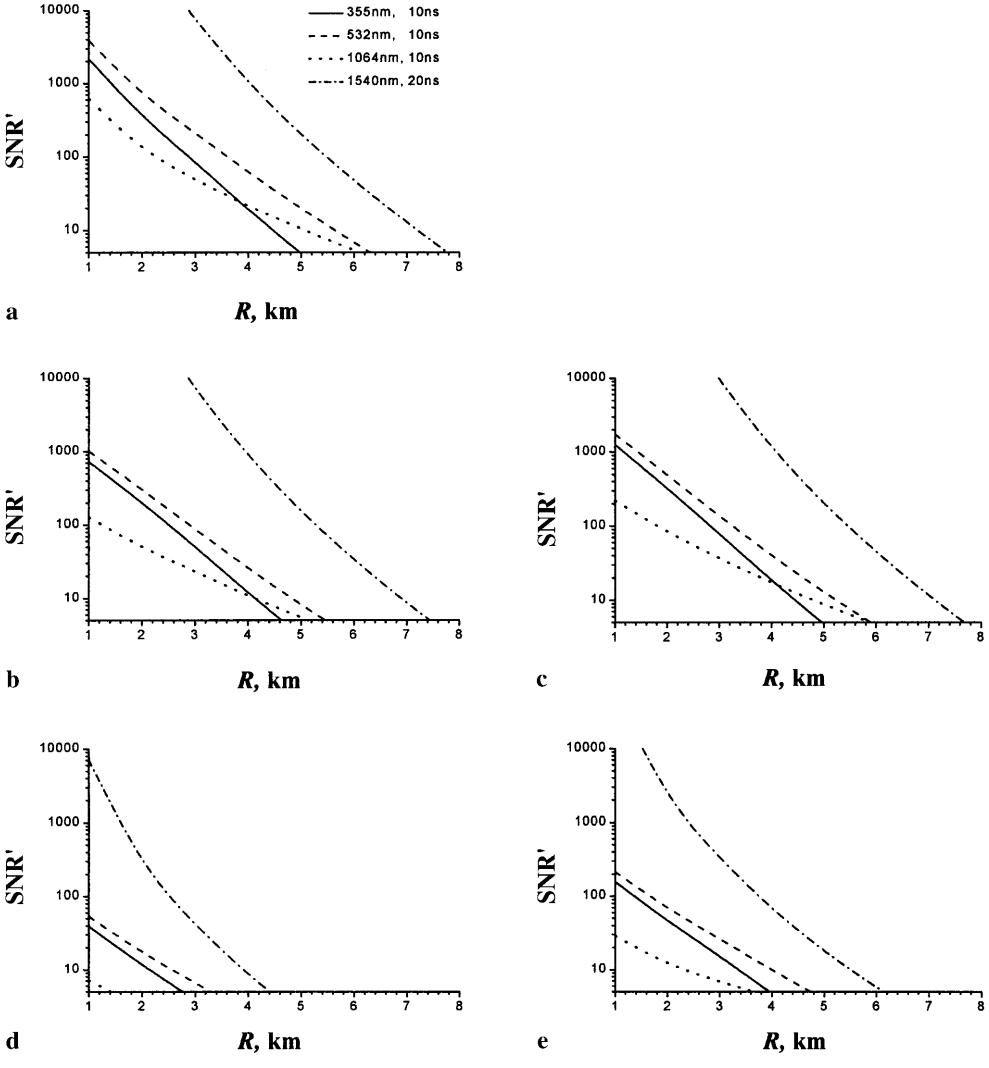

FIGURE 3 Variation of SNR′ with distance. Laser beam divergence 2.5 mr, burning rate 0.05 kg/s, fire radius 0.5 m. In variants shown in **a**, **b** and **d**, the integration period coincides with the pulse duration, while for **c** and **e**, the integration period is 30 and 160 ns, respectively. $z_b = 0$, 15 and 100 m for **a**, **b** and **c**, and **d** and **e**, respectively

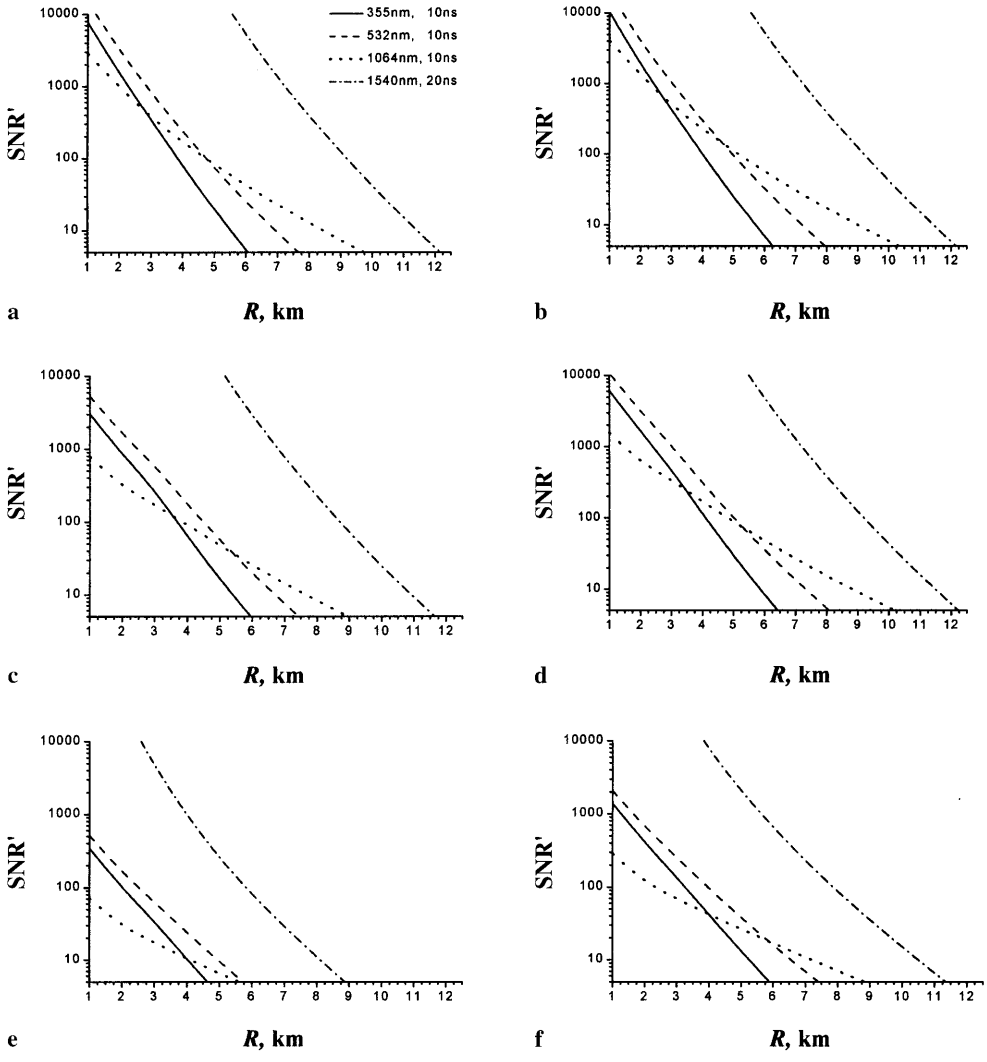

FIGURE 4 Variation of SNR′ with distance. Laser beam divergence 2.5 mr, burning rate 2 kg/s, fire radius 2.5 m. In variants shown in **a**, **c** and **e**, the integration period coincides with one laser-pulse duration. In variants shown in **b**, **d** and **f**, the integration period equals 20, 40 and 160 ns, respectively. For variants shown in **a** and **b** $z_b = 0$ m, for **c** and **d** $z_b = 15$ m, for **e** and **f** $z_b = 100$ m

creases, leading to an increase in values of SNR and SNR′. To illustrate the influence of the integration period on the SNR′(R) curve, calculation results for t_d in the interval from 20 to 160 ns are shown in Figs. 3c, 3e, 4b, 4d, 4f, 5c, 5e, and 5g. The increase in the integration period extends the detection range by 0.5 to 2 km, while an increase in the burning rate from 0.05 to 2.0 kg/s causes an extension of the detection range by 1 to 5 km, depending on the wavelength and operating conditions. This is connected with the fact that a 40-fold increase in the burning rate, provided that the fire square increases 25 times, causes an increase in the particle concentration in the plume and, consequently, a rise in the power collected by the lidar receiver. The results shown in Figs. 3 and 4 were obtained for a laser beam divergence $\gamma = 2.5$ mr. In fire surveillance applications, the choice of γ is defined by a trade-off between sensitivity and scanning speed. If γ increases, the lidar covers a larger solid angle with a single shot, decreasing surveillance time. However, for compact targets, a wider laser beam yields a lower backscattered radiation intensity, so the lidar sensitivity also decreases. The results of calculations of SNR′(R) for $\gamma = 10$ mr and various values of operational parameters are shown in Fig. 5. Comparison of these data with the curves of Figs. 3 and 4 shows that the reliable detection range for $\gamma = 10$ mr diminishes by 2 to 6 km, depending on other parameters. The explanation for this fact becomes clear after analysis of the relationship between the diameters of the plume and the laser beam at the intersection point, which is presented in Table 6. For example, at a distance of 8 km, the diameter of the area illuminated by the laser beam for $\gamma = 2.5$ and 10 mr is equal to 20 or 80 m, respectively, while the plume diameter for $z_b = 100$ m is only 30 m. This means that for $\gamma = 10$ mr, the fraction of radiation that will miss the smoke plume is several times larger than for $\gamma = 2.5$ mr and, consequently, SNR′ decreases, provided that all other factors are similar. The previous results were obtained assuming that no multiple scattering occurs, because an estimation of the influence of multiple scattering, using the results of Monte Carlo calculations carried out by Ackermann et al. [38], showed that it does not significantly affect the final results.

7 Conclusion

Using a one-dimensional "top-hat" gas dynamic model for calculation of the smoke particle concentration and the backscattering and extinction coefficient profiles within

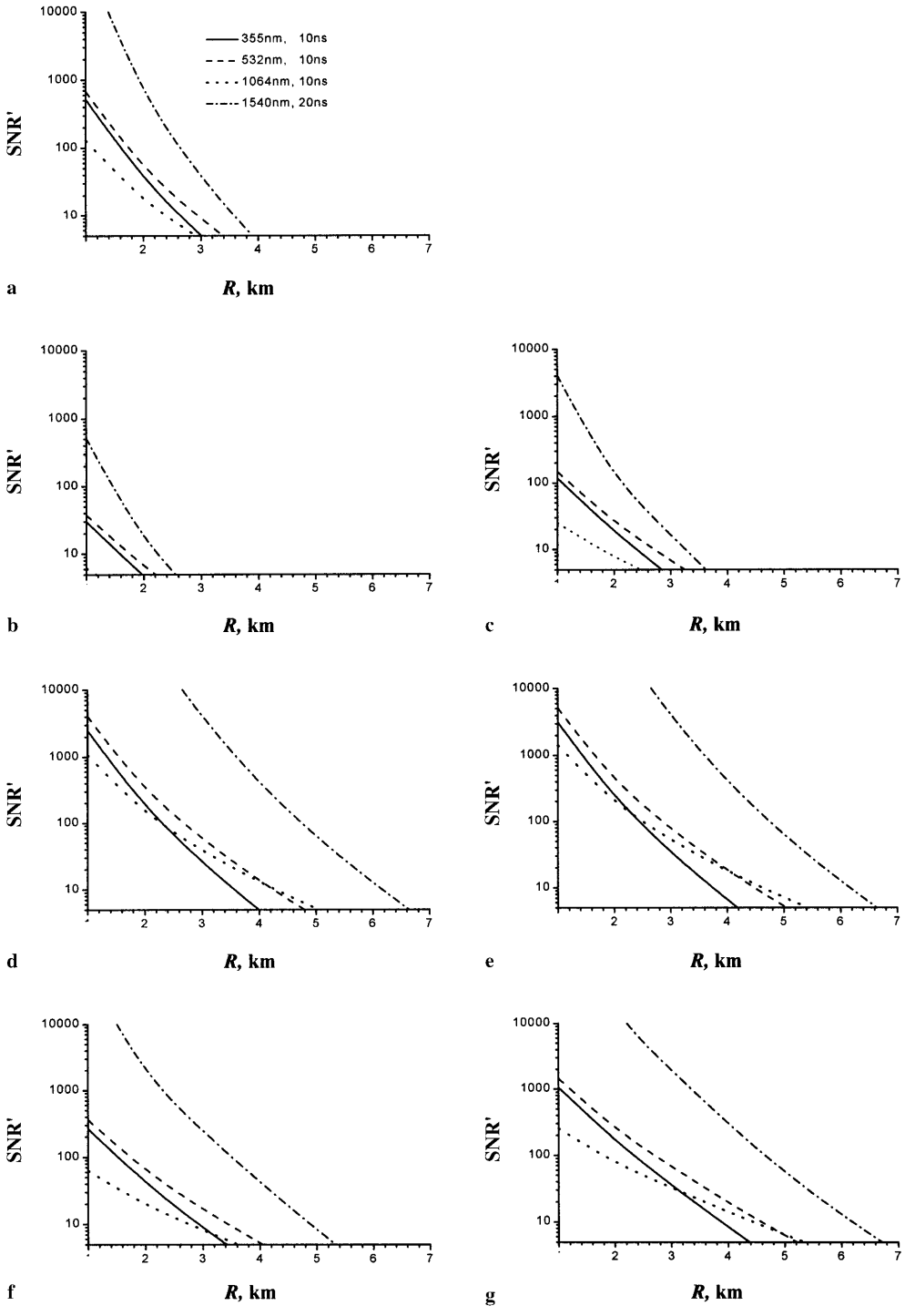

FIGURE 5 Variation of SNR′ with distance. Laser beam divergence 10 mr. In **a**, **b** and **c**, the burning rate 0.05 kg/s and the fire radius 0.5 m. In **d**, **e**, **f** and **g**, the burning rate is 2 kg/s and the fire radius is 2.5 m. In **a**, **b**, **d** and **f**, the integration period coincides with one laser-pulse duration. In **c**, **e** and **g**, the integration period is 160 ns. For **a**, **d** and **e** $z_b = 0$ m, for **b**, **c**, **f** and **g** $z_b = 10$ m

the plume, a comparison of 355, 532, 1064 and 1540-nm wavelengths was made, and on this basis the efficiency of early forest fire detection was estimated. Processing of the experimental lidar signal allowed the profile of the extinction coefficient within the plume to be restored and the smoke particle concentration along the laser beam path to be estimated. The results of the calculations show that the maximum distance for reliable forest fire detection (corresponding to $\mathrm{SNR}' = 5$) varies in the range between 1 and 12 km, depending on the operating parameters. The decrease of the signal-to-background-noise ratio with distance (using a PMT as the radiation detector) is maximum for $\lambda = 355$ nm and minimum for $\lambda = 1064$ nm. Detection at $\lambda = 1540$ nm (using an avalanche photodiode) shows slightly faster decay of SNR′ with distance. However, for all sets of the parameters used in calculations, detection at 1540 nm demonstrates higher values of SNR′ and, correspondingly, higher efficiency for the same energy of the probing laser pulse than detection at 1064 nm. For a burning rate of 2 kg/s and a laser beam divergence of 2.5 mr, the maximum distance for reliable detection varies between 6 and 12 km, depending on the wavelength.

ACKNOWLEDGEMENTS The authors wish to thank Dr.W.J. Wiscombe of the National Center for Atmospheric Research for putting at their disposal the computer program for Mie scattering calculations and Prof. X. Viegas of Coimbra University for his help in organizing the field experiments. This research was partially supported by INTAS grant No. 99-1634. A. Lavrov wishes to thank the NATO Scientific Affairs Division for a fellowship grant, A.B. Utkin gratefully acknowledges financial support from ICEMS, and A. Fernandes acknowledges a Ph.D. grant from the Portuguese Fundação para a Ciência e a Tecnologia.

REFERENCES

1 F. Andreucci, M.V. Arbolino: Nuovo Cimento **16C**, 35 (1993)
2 F. Andreucci, M.V. Arbolino: Nuovo Cimento **16C**, 51 (1993)
3 A. Lavrov, R. Vilar: Proc. SPIE **3868**, 473 (1999)
4 S. Pershin, W.M. Hao, R.A. Susott, R.E. Babbitt, A. Riebau: Proc. SPIE **3757**, 60 (1999)
5 R. Vilar, A. Lavrov: Appl. Phys. B **71**, 225 (2000)
6 P.J. Thomas, O. Nixon: Appl. Opt. **32**, 5348 (1993)
7 Y. Rauste, E. Herland, H. Frelander, K. Soini, T. Kuoremaki, R. Ruokari: Int. J. Remote Sensing **18**, 2641 (1997)
8 W. Carnuth, T. Trickl: Rev. Sci. Instrum. **65**, 3324 (1994)
9 IEC 825–1: 1993, Safety of Laser Products – Part 1: Equipment Classification Requirements and User's Guide (International Electrotechnical Commission, Geneva, Switzerland 1993)
10 D.G. Youmans, R. Garner, K.R. Peterson: Proc. SPIE **2271**, 13 (1994)
11 W.L. Eberhard: Appl. Opt. **22**, 2282 (1983)
12 J.L. Stith, L.F. Radke, P.V. Hobbs: Atmos. Environ. **15**, 73 (1981)
13 J.S. de Vries, E. den Breejen: Proc. SPIE **1968**, 716 (1993)
14 C. Hueglin, C. Gaegauf, S. Kunzel, H. Burtscher: Envir. Sci. Technol. **31**, 3439 (1997)
15 B.R. Morton: In: 10th Symp. (Int.) on Combustion (The Combustion Institute, Pittsburgh 1965) p. 973
16 B.R. Morton, G. Taylor, J.S. Turner: Proc. Roy. Soc. (London) A **234**, 1 (1956)
17 A. Askari, S.J. Bullman, M. Fairweather, F. Swaffield: Combust. Sci. Technol. **73**, 463 (1990)
18 R.M. Measures: *Laser Remote Sensing* (Wiley, New York 1984)
19 J.A. Overbeck, M.S. Salisbury, M.B. Mark, E.A. Watson: Appl. Opt. **34**, 7724 (1995)
20 A.B. Utkin, A.V. Lavrov, L. Costa, F. Simões, R. Vilar: Appl. Phys. B **74**, 77 (2002)
21 D. Althausen, D. Muller, A. Ansmann, U. Wandinger, H. Hube, E. Clauder, S. Zorner: J. Atmos. Ocean. Technol. **17**, 1469 (2000)
22 Z. Liu, P. Voelger, N. Sugimoto: Appl. Opt. **39**, 3120 (2000)
23 E.M. Patterson, C.K. McMahom: Atmos. Environ. **18**, 2541 (1984)
24 J.V. Martins, P.V. Hobbs, R.E. Weiss, P. Artaxo: J. Geophys. Res. **103**, 32051 (1998)
25 J.D. Klett: Appl. Opt. **20**, 211 (1981)
26 E. Durieux, L. Fiorani: In: Instrument Development for Atmospheric Research and Monitoring (Springer, Berlin 1997) p. 89
27 B. Nilsson: Appl. Opt. **18**, 3457 (1979)
28 B. Benech, P.V. Dinh, A. Ezcurra, J.L. Lesne: Atmos. Environ. **22**, 1071 (1988)
29 L.R. Bissonnette: Appl. Opt. **25**, 2122 (1986)
30 W.J. Wiscombe: Appl. Opt. **19**, 1505 (1980)
31 D.X. Viegas, P.R. Ribeiro, M.G. Cruz: In: Proc. 3rd Int. Conf. on Forest Fire Research, Vol. 1–2 (University of Coimbra, Coimbra, Portugal 1998) p. 467
32 P.M. Fernandes: In: Proc. 3rd Int. Conf. on Forest Fire Research, Vol. 1–2 (University of Coimbra, Coimbra, Portugal 1998) p. 611
33 M.G. Cruz, D.X. Viegas: In: Proc. 3rd Int. Conf. on Forest Fire Research, Vol. 1–2 (University of Coimbra, Coimbra, Portugal 1998) p. 859
34 M.C. Alves: In: Proc. 3rd Int. Conf. on Forest Fire Research, Vol. 1–2 (University of Coimbra, Coimbra, Portugal 1998) p. 1047
35 W.K. Pratt: *Laser Communication Systems* (Wiley, New York 1969)
36 E. Georgiou, O. Musset, J.P. Boquillon: In: Conf. Digest, 2000 Conf. on Lasers and Electro-Optics Europe, Nice, France (IEEE Catalog Number: 00TH8505 2000) p. 51
37 R. Wu, J.D. Myers, M.J. Myers: Proc. SPIE **3707**, 342 (1999)
38 J. Ackermann, P. Volger, M. Wiegner: Appl. Opt. **38**, 5195 (1999)